





Article

Enhanced Thermal Stability in Dielectric Properties of NaNbO_3 -Modified BaTiO_3 - $\text{BiMg}_{1/2}\text{Ti}_{1/2}\text{O}_3$ Ceramics for X9R-MLCC Applications

Raz Muhammad ^{1,*}, Asif Ali ¹, Javier Camargo ², Miriam S. Castro ², Wen Lei ^{3,4}, Kaixin Song ⁵ and Dawei Wang ^{6,*}

¹ Department of Physics, Garden Campus, Abdul Wali Khan University Mardan, Mardan 23200, KP, Pakistan; asif.lfmd@gmail.com

² Institute of Research in Materials Science and Technology, National University of Mar del Plata, Av. Colon 10850, Mar del Plata B7606BVZ, Argentina; jcamargo@fi.mdp.edu.ar (J.C.); mcastro@fi.mdp.edu.ar (M.S.C.)

³ Wenzhou Advanced Manufacturing Technology Research Institute, Huazhong University of Science and Technology, Wenzhou 325035, China; wenlei@mail.hust.edu.cn

⁴ School of Optical and Electronic Information, Huazhong University of Science and Technology, Wuhan 430074, China

⁵ College of Electronics Information, Hangzhou Dianzi University, Hangzhou 310018, China; kxsong@hdu.edu.cn

⁶ Shenzhen Institute of Advanced Electronic Materials, Shenzhen Institute of Advanced Technology, Chinese Academy of Sciences, Shenzhen 518055, China

* Correspondence: raz@awkum.edu.pk (R.M.); wangdawei102@gmail.com (D.W.)



Citation: Muhammad, R.; Ali, A.; Camargo, J.; Castro, M.S.; Lei, W.; Song, K.; Wang, D. Enhanced Thermal Stability in Dielectric Properties of NaNbO_3 -Modified BaTiO_3 - $\text{BiMg}_{1/2}\text{Ti}_{1/2}\text{O}_3$ Ceramics for X9R-MLCC Applications. *Crystals* **2022**, *12*, 141. <https://doi.org/10.3390/cryst12020141>

Academic Editors: Sergio Brutti and Alexei A. Bokov

Received: 5 January 2022

Accepted: 18 January 2022

Published: 19 January 2022

Publisher's Note: MDPI stays neutral with regard to jurisdictional claims in published maps and institutional affiliations.



Copyright: © 2022 by the authors. Licensee MDPI, Basel, Switzerland. This article is an open access article distributed under the terms and conditions of the Creative Commons Attribution (CC BY) license (<https://creativecommons.org/licenses/by/4.0/>).

Abstract: $0.5\text{BaTiO}_3-(0.5-x)\text{BiMg}_{1/2}\text{Ti}_{1/2}\text{O}_3-x\text{NaNbO}_3$ ($x = 0.10-0.30$) ceramics were processed via a conventional solid state sintering route. X-ray diffraction analysis and Raman spectroscopy showed the formation of a cubic perovskite structure. Microstructural analysis of the samples revealed densely packed grains. The addition of NaNbO_3 resulted in the enhancement in dielectric properties as a function of temperature. Relative permittivity decreased from 850 to 564 (at room temperature) with an increase in x ; however, the stability in dielectric properties was improved with an increase in NaNbO_3 concentration. At $x = 0.25$, relative permittivity (ϵ_r) was $\sim 630 \pm 15\%$ in a temperature range of $-70-220^\circ\text{C}$ with low dielectric loss ($\tan \delta$) < 0.025 (-57 to 350°C) and high recoverable energy density $\sim 0.55\text{ J/cm}^3$ which meet the criterion for X9R MLCC applications.

Keywords: BaTiO_3 ; capacitor; dielectric properties; X9R

1. Introduction

The electronic industry is growing rapidly and demands new materials with improved performance for various applications. Among the electronic components, the capacitor is one of the most widely used components for both low temperature, as well as harsh environment applications [1–4]. The present market of ceramic capacitors is dominated by the multi-layer ceramic capacitor (MLCC), having the advantages of both high volumetric efficiency and small size [5–7]. Trillions of pieces are fabricated every year which makes it one of the most widely used components used in electronic circuits [8]. The major characteristics required for capacitor applications are temperature stable high relative permittivity (ϵ_r), high breakdown strength (BDS) and low dielectric loss ($\tan \delta$) [9]. The Electrical industries association designated the upper and lower working temperature limit for the ceramic capacitor as X7R, X8R and X9R, where 'X' represents the lower working temperature limit which is -55°C , the mid digit stands for 125, 150 and 200°C temperature for 7, 8 and 9, respectively and 'R' represents minimum variation in the capacitance value (i.e., $\pm 15\%$) [10,11]. On the other hand, for high temperature electronics (HTE),

the electronic equipment has to operate at a high temperature greater than >200 °C. For example, the electronic anti-lock brake system on wheels operates across the temperature range of 150–250 °C, some parts working near the engine operate near 200–300 °C and some other applications, such as down-hole drilling and aerospace [12–15].

High ϵ_r dielectrics are preferred for capacitors and there are some promising lead-based ceramics that have a high ϵ_r value in the range of 10,000–25,000, such as $\text{Pb}(\text{Fe}_{1/3}\text{W}_{2/3})\text{O}_3$, $\text{Pb}(\text{Mg}_{1/3}\text{Nb}_{2/3})\text{O}_3$ and $\text{Pb}(\text{Zn}_{1/3}\text{Nb}_{2/3})\text{O}_3$ but lead is considered toxic and hazardous to human health [16–23]. Therefore, the use of lead is constrained by the European Union. Thus, BaTiO_3 (BT) remains the only choice that is considered as a cornerstone for the fabrication of the ceramic capacitor. BT has a perovskite structure and accommodates many cations at both the A- and B-site [24,25]. In industrial applications, Ho^{3+} and Eu^{3+} doped BT is used in MLCCs for X7R and X8R applications; however, the operating temperature windows need to be extended. The major problem with the pure BaTiO_3 is a sharp Curie temperature (T_c) near 120 °C and a high sintering temperature ~ 1350 °C. Generally, Bi-based perovskites are useful in lowering sintering temperature and broadening of T_c [26–28]. The binary solid solution $(1-x)\text{BaTiO}_3-x\text{Bi}(\text{Mg}_{2/3}\text{Nb}_{1/3})\text{O}_3$ (BT- x BMN) ceramics has been reported [29] to possess a temperature-stable relative permittivity of $\epsilon_r = 940 \pm 15\%$ across 34 to 550 °C and $\tan \delta < 0.025$ (74–455 °C). Among such binary solid solutions, $(1-x)\text{BaTiO}_3-x\text{BiMg}_{1/2}\text{Ti}_{1/2}\text{O}_3$ (BT-BMT) was extensively investigated, and therefore, is of great interest [30–37]. Zhang et al. [30] investigated BT- x BMT solid solution for $x = 0$ to 0.8 and reported high ϵ_r values (1500–3000) which attracted considerable attention from researchers. Besides, NaNbO_3 -modified 0.75BT-0.25BMN which exhibited $\epsilon_r = 840 \pm 15\%$ in the temperature range of -62 to 192 °C with low $\tan \delta < 2\%$ across -28 –374 °C was reported by the authors [38]. Still, BT-BMT-based ceramics are of great interest for capacitors and high energy density storage applications [39–41]. Recently, La-modified BT-BMT was reported to exhibit $\epsilon_r = 572 \pm 15\%$ over the temperature range -70 –238 °C [42]. The addition of NaNbO_3 (NN) was very useful in extending temperature stability below room temperature and energy storage applications [43,44]. In the present study, we report the enhanced performance of BT-BMT by substituting Na^+ and Nb^{5+} in the host lattice.

2. Materials and Methods

$0.5\text{BaTiO}_3-(0.5-x)\text{BiMg}_{1/2}\text{Ti}_{1/2}\text{O}_3-x\text{NaNbO}_3$ (BT-BMT-NN) ceramics with $x = 0.10$ –0.30 were processed through a solid-state sintering route. Reagent grade (purity $> 99\%$, Sigma Aldrich) raw chemicals BaCO_3 , Bi_2O_3 , TiO_2 , MgO , Na_2CO_3 and Nb_2O_5 were dried to remove moisture and hydroxides and then weighted according to the molar ratios of batches. Powders were mixed/milled using a planetary ball mill (Fritsch, pulverisette 7600 rpm, Germany) in isopropanol for 6 h. The mixed powders were calcined at 900 °C for 4 h and then re-milled to dissociate agglomerates. The calcined powders were pressed into cylindrical shape pellets using a 10 mm die, at a pressure of 100 MPa and sintered in the temperature range 1050–1125 °C for 2 h.

The density of sintered samples was measured by the Archimedes principle. Phase analysis was carried out at room temperature using a PANalytical X'pert Pro X-ray diffractometer (United Kingdom), using $\text{CuK}\alpha$ radiations. Raman spectra of the samples were collected at room temperature using a Renishaw In Via Reflex microspectrometer (United Kingdom), using a 514 nm Ar laser at a power between 30 and 300 mW. The samples were thermally etched at a temperature 10% lower than the sintering temperature (990 °C for 15 min). The microstructure of the polished and thermally etched samples was analyzed using a JEOL (JSM-6460LV) scanning electron microscope (Japan). For electrical measurements, pellets were coated with silver on both sides. Dielectric properties as a function of temperature were measured using an Agilent 4284A LCR meter (United States). Capacitance (C_p) and $\tan \delta$ were measured at 1 kHz, 10 kHz, 100 kHz and 1 MHz in the temperature range from -70 to 500 °C. Low-temperature data were collected in liquid

nitrogen using a homemade system. Polarization-electric field (P-E) loops were measured at a frequency of 10 Hz, using a modified Sawyer–Tower circuit at room temperature.

3. Results

X-ray diffraction (XRD) patterns of BT–BMT–NN, sintered at 1100 °C for 2 h are shown in Figure 1a. The diffraction patterns matched JCPDS # 131-0174, having a cubic perovskite structure and the patterns were indexed accordingly. No evidence of secondary peaks was observed within the detection limit of the in-house XRD facility, suggesting that Na and Nb cations were completely soluble in the BT–BMT solid solution. The peaks slightly shifted to high 2θ values (higher d-spacings), indicating a decrease in unit cell volume, which may be due to the replacement of slightly larger Bi ions ($r_{\text{XII}} = 1.38 \text{ \AA}$) by Na ions ($r_{\text{XII}} = 1.34 \text{ \AA}$) at the A-site, and Mg ions ($r_{\text{VI}} = 0.72 \text{ \AA}$) by Nb ions ($r_{\text{VI}} = 0.64 \text{ \AA}$) at the B-site of the host lattice [45]. Figure 1b shows the enlarged view of (200) reflection which shows no splitting, indicating the cubic-like structure.

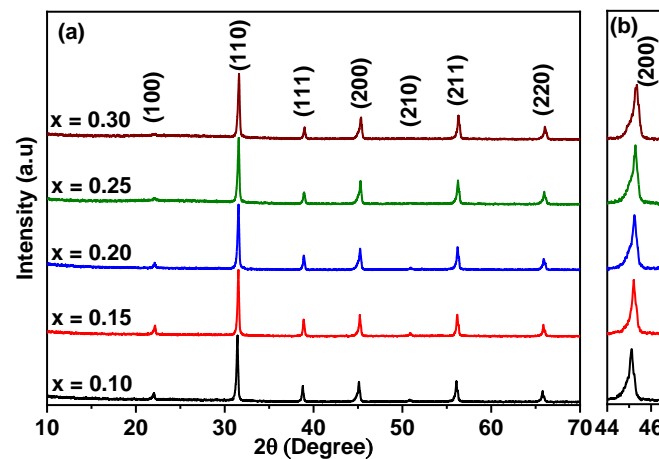


Figure 1. (a) XRD patterns of BT–BMT–NN ceramics, sintered at 1100 °C for 2 h, (b) enlarged (200) peak.

For a better understanding of the local structure, room temperature Raman spectra of BT–BMT–NN ceramics were recorded as shown in Figure 2, which is consistent with the data previously reported for BT–BMT [34]. The Raman bands were overlapped and became broader with the increase of NN content, indicating the disorder in the lattice induced by the multiple ions at the same site [46]. For a better illustration, the Raman spectrum was fitted using a simple Lorentzian function, as shown in Figure 2. The first sharp peak at 117 cm^{-1} and the second band near 180 cm^{-1} was related to vibrations of A-site cations and displacement [47]. The band near 180 cm^{-1} shifted to lower wavenumber, probably due to the incorporation of Na^+ for Bi^{3+} with different ionic sizes [45]. In pure BT, a sharp peak appears near 305 cm^{-1} along with a dip near 180 cm^{-1} which is indicative of long-range ferroelectric order. In the present case, a relatively broader band at 335 cm^{-1} and another band near 281 cm^{-1} appeared (polar BO_6 octahedral vibrations), and starts merging with increasing x -value [48]. This behavior may be associated with the destruction of ferroelectric order and the broadening may be related to the formation of polar-nano regions due to multiple cations at the same site of the lattice. The Raman bands in the range 400 to 650 cm^{-1} are often related to the vibrations of oxygen octahedrons [46]. In the present case, two different bands at 497 and 575 cm^{-1} were observed which merged with an increase in x . The possible reason for this behavior may be the stretching symmetric vibrations of TiO_6 and MgO_6 octahedra because ionic radii difference is large between Ti^{4+} and Mg^{2+} . The substitution of Nb^{5+} resulted in a broad band which may be due to decreasing amount of Mg^{2+} because the ionic radii difference between Nb^{5+} and Ti^{4+} is small. The modes at 724 and 773 cm^{-1} merged to form a broad band. This band is known as A1g mode which is associated with the breathing of BO_6 octahedra [49]. A1g mode is symmetric and Raman active in A-site doped BT but the splitting comes from the different

octahedra because the frequency of this mode changes with change in ionic radius which creates asymmetry [50].

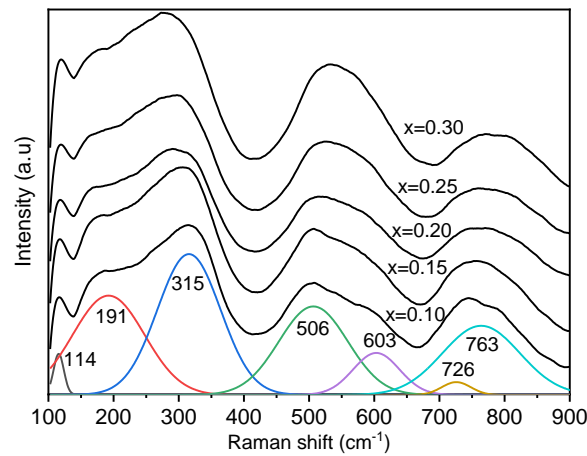


Figure 2. Raman spectra of BT-BMT-NN ceramics.

The samples were sintered in the temperature range 1050–1125 °C for 2 h (Figure 3a). For all samples, the bulk density increased with an increase in temperature from 1050 °C. For a sample with $x = 0.10$, maximum bulk density was observed at 1075 °C which decreased with a further increase in temperature. For samples with $x > 0.10$, the highest bulk density was observed at a sintering temperature of 1100 °C. The decrease in bulk density above optimal sintering temperature may be due to the volatile nature of bismuth or abnormal grain growth. However, for a better comparison, the samples sintered at 1100 °C (optimal sintering temperature) were selected for investigation because bismuth is volatile and a slight temperature change may affect the properties of the sintered ceramics. Figure 3b shows a variation in bulk density versus x (NaNbO_3 concentration). The bulk density decreased with an increase in x which may be due to the decreasing amount of bismuth as the atomic weight of bismuth is higher than sodium.

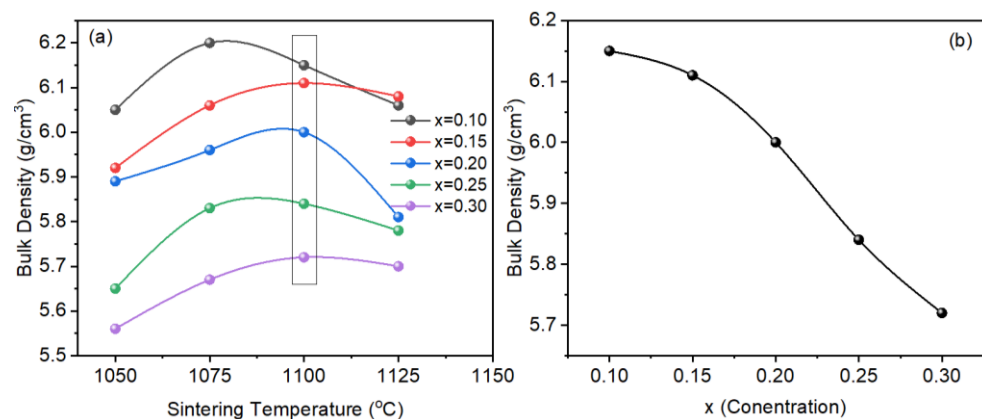


Figure 3. Bulk density versus (a) temperature, and (b) NaNbO_3 concentration (x) in BT-BMT.

Figure 4 shows the SEM images of the polished and thermally etched BT-BMT-NN ceramics sintered at 1100 °C for 2 h. All the samples showed well-packed grains and dense microstructure, consistent with the high relative density (>94%). The average grain size was found to be quite small of 1–1.8 μm for samples with $x = 0.10$ to 0.30 (See Supplementary Materials Figure S1), which is, technologically, of great importance for the fabrication of MLCCs [51]. The average grain size and relative density of all the samples sintered at 1100 °C are given in Table 1. For a sample with $x = 0.25$, both the relative density and grain size were larger.

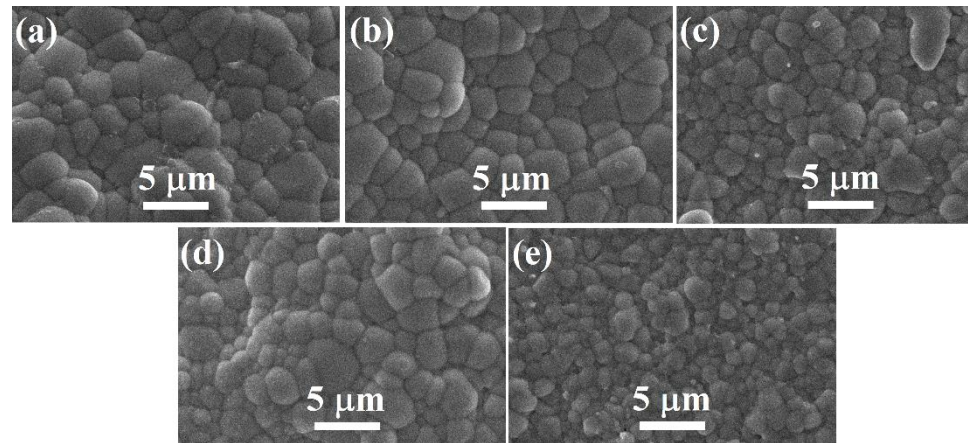


Figure 4. SEM micrographs of BT-BMT-NN ceramics for $x =$ (a) 0.10, (b) 0.15 (c) 0.20 (d) 0.25 and (e) 0.30 sintered at 1100 °C.

Table 1. Relative density and average grain size of BT-BMT-NN ceramics.

x	Relative Density (%)	Average Grain Size (μm)
0.1	96.0	1.8
0.15	96.8	1.77
0.2	94.4	1.20
0.25	97.8	1.44
0.3	96.5	1.06

The ϵ_r and $\tan \delta$ as a function of temperature for BT-BMT-NN ceramics measured at different frequencies from 1 kHz–1 MHz in a temperature range of -70 to 500 °C is shown in Figure 5a–e. The temperature of maximum ϵ_r (T_m) drastically decreased from 91 to -40 °C, with an increase in x from 0.10 to 0.30. A similar effect of decreasing T_m was reported for NaNbO_3 -modified BaTiO_3 - $\text{Bi}(\text{Zn}_{0.5}\text{Ti}_{0.5})\text{O}_3$ solid solution [52]. ϵ_r linearly decreased with an increase in Na^+ and Nb^{5+} concentration which encouraged the short-range ferroelectric behavior. A similar trend was observed for $(1-x)\text{NaNbO}_3$ - $x\text{BaTiO}_3$ ceramics [53]. Another reason for the decrease in ϵ_r may be the smaller polarizability of Nb^{5+} than Ti^{4+} . As evident from the P-E loops and Raman data, the crystal structure is cubic but still, ϵ_r is higher than centrosymmetric structures, such as CaTiO_3 which may be attributed to the formation of polar nanoregions (PNRs) due to the occupancy of multiple cations at the same site [31].

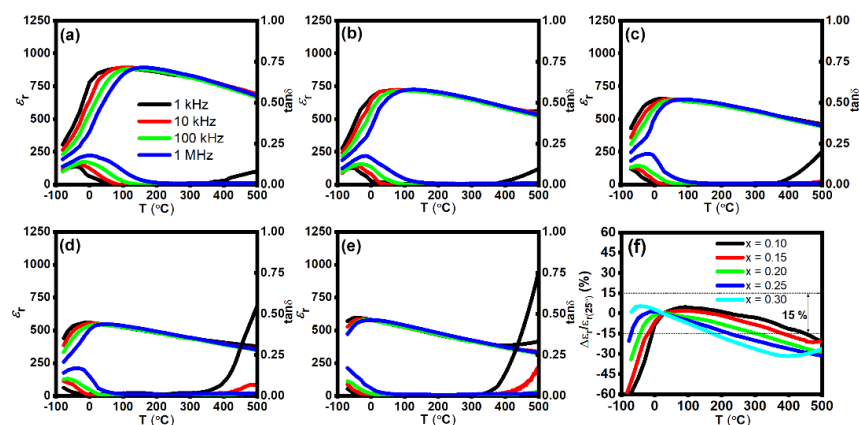


Figure 5. ϵ_r and $\tan \delta$ as a function of temperature for $x =$ (a) 0.10, (b) 0.15, (c) 0.20, (d) 0.25, (e) 0.30, and (f) variation in ϵ_r as a function of temperature for BT-BMT-NN ceramics.

T_m shifted to a lower temperature and the thermal stability of ϵ_r was enhanced with the increase of NN content. Dielectric properties of BT–BMT–NN ceramics are listed in Table 2 while the variation in ϵ_r as a function of temperature is shown in Figure 5f. The sample with $x = 0.10$ possesses $\epsilon_r = 850 \pm 15\%$ across -8 to 450 °C and $\tan \delta < 0.025$ (25 – 412 °C). Upon further increase in x , lower temperature stability was enhanced below room temperature, but high temperature stability degraded. An optimum set of dielectric properties were achieved for $x = 0.25$, i.e., $\epsilon_r = 630 \pm 15\%$ stable over the temperature range -70 °C to 220 °C, and the dielectric loss was < 0.25 over the operating temperature range -57 – 350 °C which satisfy the requirements of the X9R type capacitor.

Table 2. Dielectric properties of BT–BMT–NN ceramics.

x	T_m (°C)	$\epsilon_{r(\max)}$	$\epsilon_{r(\text{RT})}$	T-Range (°C) $\epsilon_{r(\text{RT})} \pm 15\%$ (1 kHz)	T-Range (°C) $\tan \delta < 0.025$ (1 kHz)	Ref.
0.1	~91	890	850	–8–450	25–412	This work
0.15	<66	722	710	–20–390	–3–418	
0.2	<28	656	655	–43–305	–26–400	
0.25	0	641	630	–70–220	–57–350	
0.3	–40	593	565	–70–165	–62–357	
Nb-doped BT-BMT	–	–	764	–55–200	~–25–200	[36]
La-doped BT-BMT	0	>500	572	–70–238	–40–300	[42]
BT–BiYO ₃	~50		417	–55–200	100–200 (<0.01)	[54]
BNT–SrZrO ₃ –NN	–	1250	1170	–55–545	–55–300	[55]

A dispersion below T_m was observed which is indicative of the “relaxor behavior”. The relaxor behavior of ferroelectric materials can be effectively described with the help of modified Curie–Weiss law [56,57].

$$\frac{1}{\epsilon} - \frac{1}{\epsilon_m} = \frac{(T - T_m)^\gamma}{C} \quad (1)$$

Here, ‘ ϵ_m ’ represents maximum ϵ_r , ‘ γ ’ and ‘ C ’ are constants. The value γ varies from 1–2 for normal to ideal relaxor ferroelectrics. γ is obtained from the slope of $\log(1/\epsilon - 1/\epsilon_m)$ versus $\log(T - T_m)$ as plotted in Figure 6. The value γ ranges from 1.32 to 1.54, indicating relaxor-like behavior. It has been reported [48,58] that cation disorder at the A- and/or B-site is responsible for relaxor behavior, in agreement with the Raman studies (Figure 2).

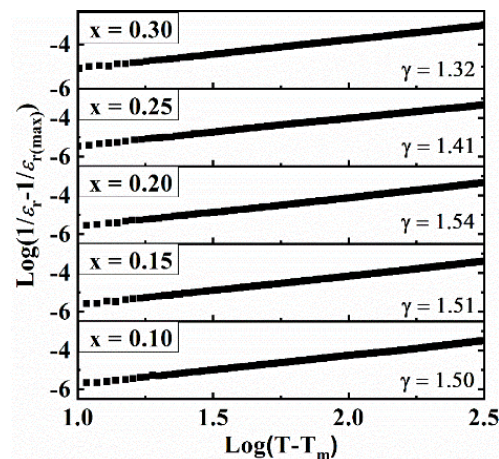


Figure 6. The plot of $\log(1/\epsilon - 1/\epsilon_m)$ versus $\log(T - T_m)$ for BT–BMT–NN ceramics at 1 MHz.

Figure 7 shows P-E loops for BT-BMT-NN samples measured at 75 kV/cm. The samples with $x = 0.30$ exhibited the lowest maximum polarization, $P_m = 3.43 \mu\text{C}/\text{cm}^2$ while the maximum P_m value of $6.4 \mu\text{C}/\text{cm}^2$ was obtained for samples with $x = 0.10$. Similar behavior was observed in Na^+ and Nb^{5+} doped $\text{Bi}_{0.5}\text{Na}_{0.5}\text{TiO}_3$ -BT ceramics [59]. The decrease in polarization may be due to the decrease in polarizability of the constituents. However, a non-linear trend was observed in P_m values for samples with $x = 0.2$ and 0.25 . For both these two samples, an opening in the P-E loops was also observed which shows a weakly nonlinear dielectric behavior. The same phenomenon was observed for $(1-x)\text{BT}-x\text{BMT}$ ($x = 0.4$) ceramics which was attributed to the increase in the conductive $\tan \delta$ at room temperature [33]. For BT-BMT-NN with $x = 0.20$ and 0.25 , $\tan \delta$ is very low (<0.025) at room temperature; therefore, the origin for the observed weak non-linear behavior needs further investigation. The recoverable energy density (W_{rec}) calculated for the sample with $x = 0.10$ was $0.5 \text{ J}/\text{cm}^3$ at an applied electric field of $110 \text{ kV}/\text{cm}$. A maximum W_{rec} of $0.55 \text{ J}/\text{cm}^3$ and an efficiency of 82% were observed for the sample with $x = 0.25$ at $150 \text{ kV}/\text{cm}$.

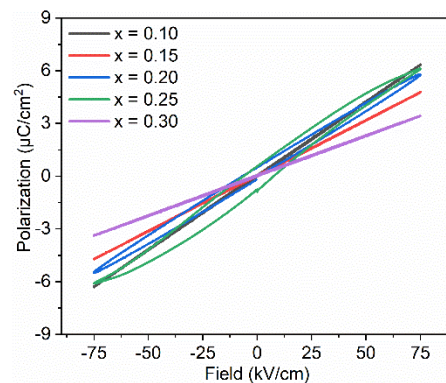


Figure 7. Hysteresis loops for BT-BMT-NN ceramics.

4. Conclusions

$0.5\text{BaTiO}_3-(0.5-x)\text{BiMg}_{1/2}\text{Ti}_{1/2}\text{O}_3-x\text{NaNbO}_3$ ($x = 0.10-0.30$) lead-free ceramics were prepared which form a single phase cubic perovskite structure, indicating that Na^+ and Nb^{5+} are soluble in the host lattice. Although the samples have a paraelectric phase, the high ϵ_r was due to the formation of nano-polar regions, confirmed from the Raman spectra of the samples. Microstructural analysis shows that dense ceramics of the solid solution could be easily prepared by a solid state route. The samples exhibited a flat temperature dependent response. Optimum dielectric properties were observed for the sample with $x = 0.25$ i.e., $\epsilon_r = 630 \pm 15\%$ over the temperature range from $-70-220 \text{ }^\circ\text{C}$ and $\tan \delta < 2.5\%$ over -57 to $350 \text{ }^\circ\text{C}$, suggesting that it is a promising candidate material for the X9R capacitor.

Supplementary Materials: The following supporting information can be downloaded at: <https://www.mdpi.com/article/10.3390/cryst12020141/s1>, Figure S1: Histogram of grain size distribution.

Author Contributions: Conceptualization, R.M. and M.S.C.; methodology, R.M. and J.C.; software, A.A. and J.C.; validation, W.L., K.S. and D.W.; formal analysis, R.M.; investigation, R.M.; resources, M.S.C. and J.C.; data curation, J.C.; writing—original draft preparation, R.M. and A.A.; writing—review and editing, M.S.C., D.W., K.S. and W.L.; supervision, M.S.C.; project administration, M.S.C.; funding acquisition, M.S.C. All authors have read and agreed to the published version of the manuscript.

Funding: This research received no external funding.

Institutional Review Board Statement: Not applicable.

Informed Consent Statement: Not applicable.

Acknowledgments: The author (Raz Muhammad) acknowledges The World Academy of Sciences (TWAS), Italy and National Scientific and Technical Research Council (CONICET), Argentina for the research fellowship at the Institute of Materials Science and Technology (INTEMA), National University of Mar del Plata, Argentina.

Conflicts of Interest: The authors declare no conflict of interest.

References

1. Gurav, A.; Xu, X.; Freeman, Y.; Reed, E. KEMET Electronics: Breakthroughs in Capacitor Technology. In *Materials Research for Manufacturing*; Springer: Cham, Switzerland, 2016; pp. 93–129.
2. Reynolds, C. Tantalum Capacitor Technology: Options for high-temperature and harsh-environment applications. *IEEE Power Electron. Mag.* **2017**, *4*, 43–47. [[CrossRef](#)]
3. Zeb, A.; Milne, S. High temperature dielectric ceramics: A review of temperature-stable high-permittivity perovskites. *J. Mater. Sci. Mater. Electron.* **2015**, *26*, 9243–9255. [[CrossRef](#)]
4. Peddigari, M.; Palneedi, H.; Hwang, G.-T.; Ryu, J. Linear and nonlinear dielectric ceramics for high-power energy storage capacitor applications. *J. Korean Ceram. Soc.* **2018**, *56*, 1–23. [[CrossRef](#)]
5. Pan, M.-J.; Randall, C.A. A brief introduction to ceramic capacitors. *IEEE Electr. Insul. Mag.* **2010**, *26*, 44–50. [[CrossRef](#)]
6. Li, D.; Zeng, X.; Li, Z.; Shen, Z.-Y.; Hao, H.; Luo, W.; Wang, X.; Song, F.; Wang, Z.; Li, Y. Progress and perspectives in dielectric energy storage ceramics. *J. Adv. Ceram.* **2021**, *10*, 675–703. [[CrossRef](#)]
7. Wang, H.; Zhao, P.; Chen, L.; Li, L.; Wang, X. Energy storage properties of 0.87BaTiO₃-0.13Bi(Zn_{2/3}(Nb_{0.85}Ta_{0.15})_{1/3})O₃ multilayer ceramic capacitors with thin dielectric layers. *J. Adv. Ceram.* **2020**, *9*, 292–302. [[CrossRef](#)]
8. Wang, G.; Lu, Z.; Li, Y.; Li, L.; Ji, H.; Feteira, A.; Zhou, D.; Wang, D.; Zhang, S.; Reaney, I.M. Electroceramics for High-Energy Density Capacitors: Current Status and Future Perspectives. *Chem. Rev.* **2021**, *121*, 6124–6172. [[CrossRef](#)] [[PubMed](#)]
9. Morrison, F.D.; Sinclair, D.C.; West, A.R. Doping mechanisms and electrical properties of La-doped BaTiO₃ ceramics. *Int. J. Inorg. Mater.* **2001**, *3*, 1205–1210. [[CrossRef](#)]
10. Gao, S.; Wu, S.; Zhang, Y.; Yang, H.; Wang, X. Study on the microstructure and dielectric properties of X9R ceramics based on BaTiO₃. *Mater. Sci. Eng. B* **2011**, *176*, 68–71. [[CrossRef](#)]
11. Wang, S.-F.; Li, J.-H.; Hsu, Y.-F.; Wu, Y.-C.; Lai, Y.-C.; Chen, M.-H. Dielectric properties and microstructures of non-reducible high-temperature stable X9R ceramics. *J. Eur. Ceram. Soc.* **2013**, *33*, 1793–1799. [[CrossRef](#)]
12. Watson, J.; Castro, G. A review of high-temperature electronics technology and applications. *J. Mater. Sci. Mater. Electron.* **2015**, *26*, 9226–9235. [[CrossRef](#)]
13. Zhou, S.; Pu, Y.; Zhang, X.; Shi, Y.; Feng, Y.; Shen, G.; Ouyang, T.; Jia, J.; Zhang, Q.; Wang, D. High energy density, temperature stable lead-free ceramics by introducing high entropy perovskite oxide. *Chem. Eng. J.* **2022**, *427*, 131684. [[CrossRef](#)]
14. Normann, R.A. *First High-Temperature Electronics Products Survey 2005*; Sandia National Laboratories: Albuquerque, NM, USA, 2006.
15. Johnson, R.W.; Evans, J.L.; Jacobsen, P.; Thompson, J.R.; Christopher, M. The changing automotive environment: High-temperature electronics. *IEEE Trans. Electron. Packag. Manuf.* **2004**, *27*, 164–176. [[CrossRef](#)]
16. Han, Y.; Qian, J.; Yang, C. Fatigue-free dielectric capacitor with giant energy density based on lead-free Na_{0.5}Bi_{0.5}TiO₃-based film. *J. Mater. Sci. Mater. Electron.* **2019**, *30*, 21369–21376. [[CrossRef](#)]
17. Meena, V.; Dotaniya, M.L.; Saha, J.K.; Das, H.; Patra, A.K. Impact of Lead Contamination on Agroecosystem and Human Health. In *Lead in Plants and the Environment*; Springer: Berlin/Heidelberg, Germany, 2020; pp. 67–82.
18. Ibn-Mohammed, T.; Koh, S.; Reaney, I.; Sinclair, D.; Mustapha, K.; Acquaye, A.; Wang, D. Are lead-free piezoelectrics more environmentally friendly? *MRS Commun.* **2017**, *7*, 1–7. [[CrossRef](#)]
19. Ibn-Mohammed, T.; Koh, S.; Reaney, I.; Acquaye, A.; Wang, D.; Taylor, S.; Genovese, A. Integrated hybrid life cycle assessment and supply chain environmental profile evaluations of lead-based (lead zirconate titanate) versus lead-free (potassium sodium niobate) piezoelectric ceramics. *Energy Environ. Sci.* **2016**, *9*, 3495–3520. [[CrossRef](#)]
20. Wang, D.; Wang, G.; Murakami, S.; Fan, Z.; Feteira, A.; Zhou, D.; Sun, S.; Zhao, Q.; Reaney, I.M. BiFeO₃-BaTiO₃: A new generation of lead-free electroceramics. *J. Adv. Dielectr.* **2018**, *8*, 1830004. [[CrossRef](#)]
21. Xu, J.; Lu, Q.; Lin, J.; Lin, C.; Zheng, X.; Lin, T.; Wu, X. Enhanced ferro-/piezoelectric properties of tape-casting-derived Er³⁺-doped Ba_{0.85}Ca_{0.15}Ti_{0.9}Zr_{0.1}O₃ optoelectronic thick films. *J. Adv. Ceram.* **2020**, *9*, 693–702. [[CrossRef](#)]
22. Fan, Y.; Wang, Z.; Huan, Y.; Wei, T.; Wang, X. Enhanced thermal and cycling reliabilities in (K,Na)(Nb,Sb)O₃-CaZrO₃-(Bi, Na)HfO₃ ceramics. *J. Adv. Ceram.* **2020**, *9*, 349–359. [[CrossRef](#)]
23. Cen, Z.; Bian, S.; Xu, Z.; Wang, K.; Guo, L.; Li, L.; Wang, X. Simultaneously improving piezoelectric properties and temperature stability of Na_{0.5}K_{0.5}NbO₃ (KNN)-based ceramics sintered in reducing atmosphere. *J. Adv. Ceram.* **2021**, *10*, 820–831. [[CrossRef](#)]
24. Albertsen, K.; Hennings, D.; Steigelmann, O. Donor-acceptor charge complex formation in barium titanate ceramics: Role of firing atmosphere. *J. Electroceram.* **1998**, *2*, 193–198. [[CrossRef](#)]
25. Arshad, M.; Du, H.; Javed, M.S.; Maqsood, A.; Ashraf, I.; Hussain, S.; Ma, W.; Ran, H. Fabrication, structure, and frequency-dependent electrical and dielectric properties of Sr-doped BaTiO₃ ceramics. *Ceram. Int.* **2020**, *46*, 2238–2246. [[CrossRef](#)]

26. Li, W.-B.; Zhou, D.; Liu, W.-F.; Su, J.-Z.; Hussain, F.; Wang, D.-W.; Wang, G.; Lu, Z.-L.; Wang, Q.-P. High-temperature BaTiO₃-based ternary dielectric multilayers for energy storage applications with high efficiency. *Chem. Eng. J.* **2021**, *414*, 128760. [[CrossRef](#)]
27. Yang, H.; Lu, Z.; Li, L.; Bao, W.; Ji, H.; Li, J.; Feteira, A.; Xu, F.; Zhang, Y.; Sun, H. Novel BaTiO₃-based, Ag/Pd-compatible lead-free relaxors with superior energy storage performance. *ACS Appl. Mater. Interfaces* **2020**, *12*, 43942–43949. [[CrossRef](#)] [[PubMed](#)]
28. Zhao, H.; Ren, P.; Hua, Q.; Liu, L.; Wang, X.; Wan, Y.; Yan, F.; Zhao, G.; Wang, D. Temperature stable (1-x)(0.9Na_{0.5}Bi_{0.5}TiO₃-0.1BiAlO₃)-xNaTaO₃ ceramics and capacitors with ultra-wide operational range. *J. Alloys Compd.* **2021**, *886*, 161315. [[CrossRef](#)]
29. Muhammad, R.; Iqbal, Y.; Reaney, I.M. BaTiO₃-Bi(Mg_{2/3}Nb_{1/3})O₃ ceramics for high-temperature capacitor applications. *J. Am. Ceram. Soc.* **2016**, *99*, 2089–2095. [[CrossRef](#)]
30. Zhang, Q.; Li, Z.; Li, F.; Xu, Z. Structural and dielectric properties of Bi(Mg_{1/2}Ti_{1/2})O₃-BaTiO₃ lead-free ceramics. *J. Am. Ceram. Soc.* **2011**, *94*, 4335–4339. [[CrossRef](#)]
31. Sun, R.; Wang, X.; Shi, J.; Wang, L. Dielectric and polar order behaviors of BaTiO₃-Bi(Mg_{1/2}Ti_{1/2})O₃ ceramics. *Appl. Phys. A* **2011**, *104*, 129–133. [[CrossRef](#)]
32. Xiong, B.; Hao, H.; Zhang, S.; Liu, H.; Cao, M. Structure, dielectric properties and temperature stability of BaTiO₃-Bi(Mg_{1/2}Ti_{1/2})O₃ perovskite solid solutions. *J. Am. Ceram. Soc.* **2011**, *94*, 3412–3417. [[CrossRef](#)]
33. Choi, D.H.; Baker, A.; Lanagan, M.; Trolier-McKinstry, S.; Randall, C. Structural and Dielectric Properties in (1 - x)BaTiO₃-xBi(Mg_{1/2}Ti_{1/2})O₃ Ceramics (0.1 ≤ x ≤ 0.5) and Potential for High-Voltage Multilayer Capacitors. *J. Am. Ceram. Soc.* **2013**, *96*, 2197–2202. [[CrossRef](#)]
34. Ren, P.; Wang, X.; Fan, H.; Ren, Y.; Zhao, G. Structure, relaxation behaviors and nonlinear dielectric properties of BaTiO₃-Bi(Ti_{0.5}Mg_{0.5})O₃ ceramics. *Ceram. Int.* **2015**, *41*, 7693–7697. [[CrossRef](#)]
35. Muhammad, R.; Iqbal, Y. Enhanced dielectric properties in Nb-doped BT-BMT ceramics. *Ceram. Int.* **2016**, *42*, 19413–19419. [[CrossRef](#)]
36. Si, F.; Tang, B.; Fang, Z.; Zhang, S. Nb-doped 0.8BaTiO₃-0.2Bi(Mg_{0.5}Ti_{0.5})O₃ ceramics with stable dielectric properties at high temperature. *Crystals* **2017**, *7*, 168. [[CrossRef](#)]
37. Muhammad, R.; Khesro, A. Influence of A-site nonstoichiometry on the electrical properties of BT-BMT. *J. Am. Ceram. Soc.* **2017**, *100*, 1091–1097. [[CrossRef](#)]
38. Muhammad, R.; Camargo, J.; Prado, A.; Castro, M.S. Temperature stable relative permittivity from -60 to 200 °C in 75BaTiO₃-(25-x)BiMg_{0.5}Ti_{0.5}O₃-xNaNbO₃ ceramics with X9R like characteristics. *Mater. Lett.* **2018**, *233*, 258–262. [[CrossRef](#)]
39. Roncal-Herrero, T.; Harrington, J.; Zeb, A.; Milne, S.J.; Brown, A.P. Analytical Electron Microscopy Characterization of a Temperature-Stable Relaxor Ferroelectric Ceramic. *Microsc. Microanal.* **2019**, *25*, 2118–2119. [[CrossRef](#)]
40. Zeb, A.; Milne, S.J. Dielectric stability in the relaxor: Na_{0.5}Bi_{0.5}TiO₃-Ba_{0.8}Ca_{0.2}TiO₃-Bi(Mg_{0.5}Ti_{0.5})O₃-NaNbO₃ ceramic system. *Ceram. Int.* **2018**, *44*, 7663–7666. [[CrossRef](#)]
41. Xie, J.; Yao, Z.; Hao, H.; Xie, Y.; Li, Z.; Liu, H.; Cao, M. A novel lead-free bismuth magnesium titanate thin films for energy storage applications. *J. Am. Ceram. Soc.* **2019**, *102*, 3819–3822. [[CrossRef](#)]
42. Zhang, W.; Yang, J.; Wang, F.; Chen, X.; Mao, H. Enhanced dielectric properties of La-doped 0.75BaTiO₃-0.25Bi(Mg_{0.5}Ti_{0.5})O₃ ceramics for X9R-MLCC application. *Ceram. Int.* **2021**, *47*, 4486–4492. [[CrossRef](#)]
43. Zhou, M.; Liang, R.; Zhou, Z.; Dong, X. Developing a novel high performance NaNbO₃-based lead-free dielectric capacitor for energy storage applications. *Sustain. Energy Fuels* **2020**, *4*, 1225–1233. [[CrossRef](#)]
44. Shi, R.; Pu, Y.; Wang, W.; Guo, X.; Li, J.; Yang, M.; Zhou, S. A novel lead-free NaNbO₃-Bi(Zn_{0.5}Ti_{0.5})O₃ ceramics system for energy storage application with excellent stability. *J. Alloys Compd.* **2020**, *815*, 152356. [[CrossRef](#)]
45. Shannon, R.D. Revised effective ionic radii and systematic studies of interatomic distances in halides and chalcogenides. *Acta Crystallog. A* **1976**, *32*, 751–767. [[CrossRef](#)]
46. Huang, X.; Liu, H.; Song, Z.; Hao, H.; Zhang, W.; Xu, Q.; Peng, C.; Huang, L.; Cao, M. Structure–property relationships in BaTiO₃-(Na_{1/4}Bi_{3/4})(Mg_{1/4}Ti_{3/4})O₃ lead-free ceramics. *J. Eur. Ceram. Soc.* **2016**, *36*, 533–540. [[CrossRef](#)]
47. Chen, X.; Chen, J.; Ma, D.; Fang, L.; Zhou, H. Thermally stable BaTiO₃-Bi(Mg_{2/3}Nb_{1/3})O₃ solid solution with high relative permittivity in a broad temperature usage range. *J. Am. Ceram. Soc.* **2015**, *98*, 804–810. [[CrossRef](#)]
48. Ma, D.; Chen, X.; Huang, G.; Chen, J.; Zhou, H.; Fang, L. Temperature stability, structural evolution and dielectric properties of BaTiO₃-Bi(Mg_{2/3}Ta_{1/3})O₃ perovskite ceramics. *Ceram. Int.* **2015**, *41*, 7157–7161. [[CrossRef](#)]
49. Sun, Y.; Liu, H.; Hao, H.; Zhang, S. Effect of oxygen vacancy on electrical property of acceptor doped BaTiO₃-Na_{0.5}Bi_{0.5}TiO₃-Nb₂O₅ X8R systems. *J. Am. Ceram. Soc.* **2016**, *99*, 3067–3073. [[CrossRef](#)]
50. Pokorný, J.; Pasha, U.; Ben, L.; Thakur, O.; Sinclair, D.; Reaney, I. Use of Raman spectroscopy to determine the site occupancy of dopants in BaTiO₃. *J. Appl. Phys.* **2011**, *109*, 114110. [[CrossRef](#)]
51. Kishi, H.; Mizuno, Y.; Chazono, H. Base-metal electrode-multilayer ceramic capacitors: Past, present and future perspectives. *Jpn. J. Appl. Phys.* **2003**, *42*, 1. [[CrossRef](#)]
52. Raenthon, N.; Brown-Shaklee, H.; Brennecke, G.; Cann, D. Dielectric properties of BaTiO₃-Bi(Zn_{1/2}Ti_{1/2})O₃-NaNbO₃ solid solutions. *J. Mater. Sci.* **2013**, *48*, 2245–2250. [[CrossRef](#)]
53. Lu, X.; Hou, L.; Jin, L.; Wang, L.; Tian, Y.; Yu, K.; Hu, Q.; Zhang, L.; Wei, X. Structure evolution and exceptionally ultra-low hysteresis unipolar electric field-induced strain in (1 - x)NaNbO₃-xBaTiO₃ lead-free ferroelectrics. *Ceram. Int.* **2018**, *44*, 5492–5499. [[CrossRef](#)]

54. Wang, Y.; Pu, Y.; Zheng, H.; Jin, Q.; Gao, Z. Enhanced dielectric relaxation in $(1 - x)\text{BaTiO}_3-x\text{BiYO}_3$ ceramics. *Mater. Lett.* **2016**, *181*, 358–361. [[CrossRef](#)]
55. Zhu, C.; Cai, Z.; Luo, B.; Guo, L.; Li, L.; Wang, X. High temperature lead-free BNT-based ceramics with stable energy storage and dielectric properties. *J. Mater. Chem. A* **2020**, *8*, 683–692. [[CrossRef](#)]
56. Smolenskii, G.A.E. Physical phenomena in ferroelectrics with diffused phase transition. *J. Phys. Soc. Jpn.* **1970**, *28*, 26–37.
57. Uchino, K.; Nomura, S. Critical exponents of the dielectric constants in diffused-phase-transition crystals. *Ferroelectrics* **1982**, *44*, 55–61. [[CrossRef](#)]
58. Du, H.; Zhou, W.; Luo, F.; Zhu, D.; Qu, S.; Pei, Z. Phase structure, dielectric properties, and relaxor behavior of $(\text{K}_{0.5}\text{Na}_{0.5})\text{NbO}_3-(\text{Ba}_{0.5}\text{Sr}_{0.5})\text{TiO}_3$ lead-free solid solution for high temperature applications. *J. Appl. Phys.* **2009**, *105*, 124104. [[CrossRef](#)]
59. Jia, W.; Hou, Y.; Zheng, M.; Zhu, M. High-temperature dielectrics based on $(1 - x)(0.94\text{Bi}_{0.5}\text{Na}_{0.5}\text{TiO}_3-0.06\text{BaTiO}_3)-x\text{NaNbO}_3$ system. *J. Alloys Compd.* **2017**, *724*, 306–315. [[CrossRef](#)]